Short-Circuit Performance of a Synchronverter-based Microgrid

Cristian Hernández-García, *Member, IEEE*, Juan Segundo-Ramírez, *Senior Member, IEEE*, Nancy Visairo-Cruz, *Member, IEEE* and Jesús Camarillo-Montero, *Member, IEEE*

***Abstract*—Replacing synchronous generators with inverters in power grids reduces system inertia. To address this issue, the synchronconverter has been proposed as an alternative solution. This paper presents a comparative analysis of the dynamic and steady-state responses of an AC microgrid interconnected to the grid during three-phase and single-phase short-circuit events, while progressively replacing inverters with synchronverters. The results obtained show that with the incorporation of inverters with this function, the frequency deviations are smaller, the frequency oscillations are slower and the steady-state error decreases. This is compared to a system with only inverters with a conventional control law. The case study consisting of a microgrid with three inverters and interconnected to the grid was implemented in Matlab/Simulink. This study presents the incorporation of virtual inertia using the synchronverter model as a solution to the challenge of low inertia systems, a common problem when integrating renewable and intermittent energy sources into microgrids.**

Link to graphical and video abstracts, and to code: https://latamt.ieeer9.org/index.php/transactions/article/view/9238

***Index Terms*—Microgrids, synchronverter, virtual inertia, short-circuit.**

I. Introduction

THE increase of generation units based on renewable energy sources interconnected by means of power electronic converters has caused the reduction of rotational inertia levels that favor the stability of the electric power system [1]. The reduction of inertia generates that the system by its very nature is not able to store enough energy and therefore there is no energy backup during the transient process, for example, a load change or a short-circuit [2]. Under these conditions, the electrical power system is prone to lose stability, since the less energy stored, the smaller the magnitude and duration of the disturbance it will be able to withstand [2].

Microgrids based on distributed generation units, for example, are systems dominated by the phenomena and problems caused by low rotational inertia and therefore are systems prone to lose stability in case of disturbances [3], [4]. For this reason, the power electronic converters connected to the system must be able to contribute to stability and reliability, as well as make the best use of renewable resources [5].

The inertia of synchronous generators is commonly specified as the constant H, which value is proportional to the kinetic energy of the generator and inversely proportional to the rated capacity of the generator. The decrease of H in the electrical system results in an increase in the Rate of Change of Frequency (ROCOF) and higher deviations (increase of Nadir frequency) [6], [7]. This can result in tripping of components, load shedding or in the worst case scenario, cascading disconnections that can lead to the collapse of the electrical power system. [4]. Hence the concern for integrating generation sources that are not able to provide inertia to the system.

Currently, methods have been proposed to try to minimize the frequency effects of low rotational inertia, including the establishment of minimum inertia levels and/or the modification of network codes in relation to ROCOF levels that guarantee a safe operation of the electrical system [1], [8]. There are also proposals under study to increase inertia levels, e.g., by using energy storage devices and/or by incorporating synthetic or virtual inertia into converters using various measurement and control approaches, as in the case of virtual synchronous machines. [9], [10].

In most countries of the European Union, for example, a large amount of generation based on renewable sources is being incorporated, so methods and regulations are being proposed to maintain the minimum levels of inertia that guarantee the security and stability of the electricity system. ENTSO-E (European Network of Transmission System Operators Electricity's), for example, in its analysis for the future of the European power system, proposes a series of topics such as; the limitation of power flows between synchronous areas, the use of synchronous compensators, network-forming converters and fast frequency response control strategies. [1]. In the case of Ireland's EirGrid, security strategies are investigated and proposed in its network code, an example of which is to maintain a minimum inertia base in economic dispatch from auxiliary services. [1], [8]. Also, there are ROCOF limits that generators must support before a certain percentage of penetration of renewable sources. [1], [8]. Similarly, in the UK, energy storage is used to reduce inertia, and in Denmark, synchronous capacitors are used to add rotational inertia [1]. The above as actions that could contribute to the challenges when reducing the rotational inertia in the power system occurs [1], [8].

Renewable energy generation has also led to the incorpo-

The associate editor coordinating the review of this manuscript and approving it for publication was Julio Cesar Rosas-Caro (*Corresponding author: Cristian Hernández García*).

Cristian Hernández-García, and J. Camarillo-Montero are with Universidad Veracruzana, Mexico (e-mails: crishernandez@uv.mx, and jcamarillo@uv.mx).

J. S. Ramírez, and N. Visairo-Cruz are with Universidad Autónoma de San Luis Potosí, México (e-mails: juan.segundo@uaslp.mx, and nvisairoc@uaslp.mx).

ration of different topologies and modes of operation of the power system, such as DC and AC microgrids, which in most cases can be classified as low inertia systems [11], [12].

This article is based on [13], [2] y [14]. By simulating and comparing the dynamic response of the microgrid through the gradual introduction of virtual inertia, the benefits of this technique can be seen when comparing variables such as operating frequency under fault conditions. This contribution is key for the integration of renewable energies, since sources such as solar or wind do not provide inertia, and the synchronous converter model, together with energy management strategies, can help to mitigate this limitation and thus contribute positively to the stability of the system.

The objectives of this article are to:

- To perform a study of electromagnetic transients in a microgrid when inverters with conventional control law are used and synchronverters are introduced in three-phase and single-phase short-circuit conditions and at different clearing times.
- To perform a comparison of the dynamic behavior of frequency, voltage, current, power, and steady-state error in a microgrid, showing the effect of incorporating virtual inertia.

To perform the above analysis, microgrid case studies are proposed using Matlab/Simulink. short-circuit events are simulated at three different fault clearing times and under fault zone tripping and non-tripping conditions.

The present article is composed as follows: section II describes the proposed microgrid and the control law of the inverters used. Section III shows the system with the incorporation of the synchroconverter model. Section IV describes the experiments carried out and Section V presents the results and the comparison of the dynamic response of the microgrid in these experiments.

II. Study Microgrid Model

The system of study used is based on the microgrid proposed in [15], [14]. However, modifications were made in the number of generation units, magnitude of resistance and reactance of the interconnection lines and in the size of the loads. Fig. 1 shows the single-line diagram of this system, which is also used as the base case for the different simulation scenarios proposed in this research.

Specifically, the study system consists of three distributed generation units (DG1, DG2 and DG3) modeled as inverters and connected to an ideal voltage source. The connection lines between the buses of the microgrid and the common AC bus are represented by the branches RL. Linear loads are modeled on the microgrid buses, and the various Points of Common Coupling (PCCs) corresponding to each inverter are located. Additional load is added to the common bus. The operating ratings of the system are: a frequency of 60 Hz, a line RMS voltage of 440 V, and a base power of 100 kVA.
In the case of inverters, a model based on voltage sources has been used, which is described in [16], [15]. This model represents a grid-forming inverter based on a voltage and frequency reference measured at each of the PCCs. In the inverter model, $(P-\omega)$ frequency droop control is incorporated for active power control and $(Q-V)$ voltage droop control for reactive power control. The hierarchical control block diagram is shown in Fig. 2.

It can be observed that the primary control scheme is formed by an internal current control loop and an external voltage control loop, which together generate that the inverter behaves as an AC voltage source in the conversion stage. The primary control scheme is defined in the reference frame dq. On the other hand, the secondary control is devoted to generating the necessary signals to compensate for deviations at the output of the droop control, both in frequency and voltage. (Fig. 2). These signals are u_ω^{rest} and u_v^{rest}, respectively. u_ω^{rest} is the control signal for the difference between the control reference frequency ω^* and the measured frequency ω_m at the PCC. This signal is obtained from the controller PI through adjustment gains $k^{p\omega}$ and $k^{i\omega}$ as shown in the equation (1) [17].

$$u_\omega^{rest} = k^{p\omega}(\omega^* - \omega_m) + k^{i\omega}\int(\omega^* - \omega_m)dt \tag{1}$$

Similarly, u_v^{rest} s generated from the gains k^{pv} and k^{iv} and is the trim signal for the difference between the secondary control reference voltage magnitude $|V_m^{**}|$ and the measured voltage magnitude $|V_m|$. This is as shown in the equation 2 [17].

$$u_v^{rest} = k^{pv}(|V_m^{**}| - |V_m|) + k^{iv}\int(|V_m^{**}| - |V_m|)dt \tag{2}$$

Having defined the signals u_ω^{rest} and u_v^{rest}, the nominal values of frequency ω_n and voltage $|V_n|$ at the output of the inverter are obtained from the primary control as given by the equations 3 and 4 [15].

$$\omega_n = \omega^* - K^P P + u_\omega^{rest} \tag{3}$$

$$|V_n| = |V_n^*| - K^q Q + u_v^{rest} \tag{4}$$

Where the reference frequency and voltage in the primary control are ω^* and $|V_n^*|$, respectively. Similarly, K^p is the coefficient of the frequency control loop and K^q is the coefficient of the voltage control loop. P is the active power and Q is the reactive power. The K^p and K^q coefficients for each generation unit are shown in Fig. 1.

The inverter parameters and control gains used in this research are detailed in the following Table I.

III. Synchronverter Model

With the increase of distributed generation units, the inverters used are required to participate and contribute to frequency and voltage regulation and in case of fault, as mentioned in the IEEE standard 1547-2018.

One of the actions to achieve this, is to incorporate virtual synchronous machines to combine the dynamic advantages of a synchronous generator with the static characteristics of an inverter [18]. Among the virtual synchronous machines that have taken a great interest in the scientific and technological

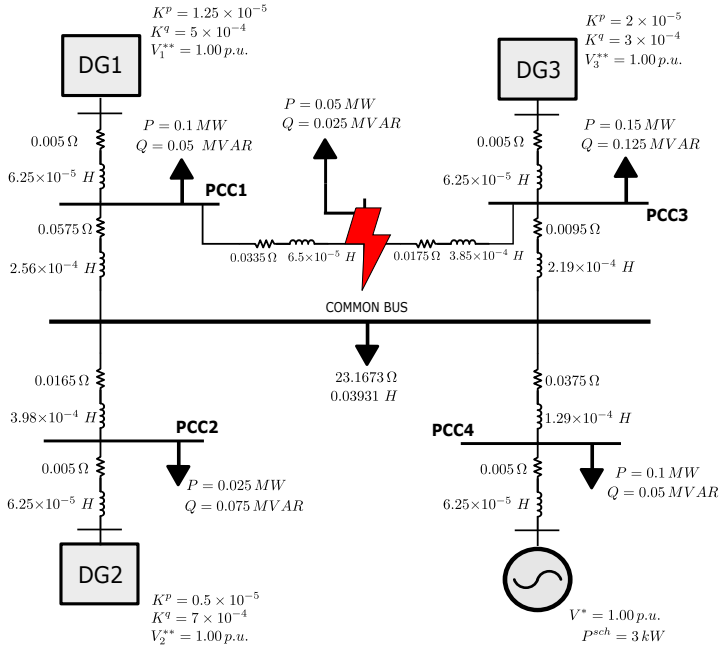

Fig. 1. Single-line diagram of the case study microgrid [15].

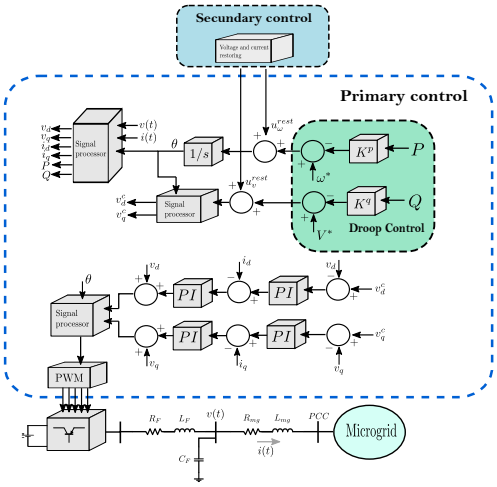

Fig. 2. Inverter hierarchical control [16], [15].

TABLE I
PROPOSED PARAMETERS OF THE INVERTER, FILTER, AND CONTROLLER FOR THE CASE STUDIES

Parameter	Symbol	Value
Rated voltage	V_{L-L}^{RMS}	440 V
Rated frequency	f	60 Hz
Rated DC voltage	v_{CD}	1500 V
Filter resistance	R_F	0.1 Ω
Filter inductance	L_F	1.8 mF
Current loop proportional gain	k_{pc}	20
Current loop integral gain	k_{ic}	40
Voltage loop proportional gain	k_{pvo}	2.4×10^{-2}
Voltage loop integral gain	k_{ivo}	4.5
Proportional gain of Freq. rest.	$k^{p\omega}$	0.02
Integral gain of Freq. rest.	$k^{i\omega}$	4
Proportional gain of voltage rest.	k^{pv}	0.2
Integral gain of Voltage rest.	k^{iv}	4
Switching frequency	f_c	10 kHz

community is the synchronverter, which mimics the behavior of a synchronous generator using a control scheme based on the mathematical model of a synchronous generator [13]. The advantages of this model include:

- As long as energy storage is available, the synchroconverter can mimic the inertial response of a real synchronous generator.
- Based on the previous point, a synchronverter is able to create virtual inertia.
- In the model, the undesirable characteristics of a real synchronous generator can be eliminated.
- Compared to some inverter control strategies, the use of the synchronverter avoids changes in control schemes when there is a transition in operating modes, for example in microgrids.
- A synchronverter contains the operating mechanisms of a real synchronous generator and therefore it is possible to benefit from the knowledge associated with its operation.
- Because it is a virtual model, parameters such as inertia and damping coefficient can be modified on-line and according to system conditions.

Therefore, by mimicking the dynamics of a synchronous generator and having virtual inertia, a synchronverter has the ability to contribute to frequency and voltage regulation during transient events, contributing to system stability [13], [19].

The model of the synchronverter used in this article is the one that was proposed in [13]. In general, this inverter combines the modeling of the electromechanical part of a synchronous generator and the operation and control characteristics of an inverter. [20], [13]. The electrical part of the synchronverter is based on a passive model of the synchronous generator, considering a round rotor, one pair of poles per phase and no damping coils [20]. In addition, the effects of

Eddy currents and magnetic saturation are not considered [13]. The moment of inertia and angular acceleration equations are the basis of the modeling for the mechanical part [13].

To describe the operation of the synchronverter, it is essential to know its structure, which in this case is composed of a power part and a control part [13]. The first refers to the structural elements of the inverter, from the DC bus to the inverter itself to the filter RLC [12], [13]. Also included are the elements necessary to obtain the voltage and current signals used to control the active and reactive power at the inverter output. [13]. The control part of the synchronverter is considered to be the most important, since it contains the control algorithms that distinguish this converter from others with a conventional control law. It is in this part that the equations considered in the electrical and mechanical modeling are incorporated in order to mimic the dynamics of a synchronous generator and, therefore, to define the generation levels of both active and reactive power [13]. As in a synchronous generator, the control strategy of the synchronverter is based on a frequency control loop for active power control and a voltage control loop for reactive power control [13]. This control structure is shown in Fig. 3.

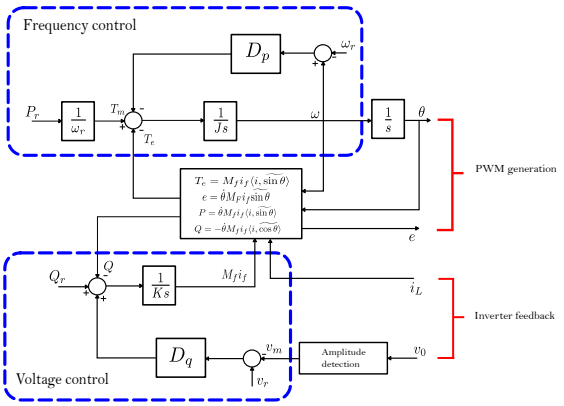

Fig. 3. Block diagram of the synchroverter's control structure [13].

From the control scheme, the equation $T_e = M_f i_f \langle i, \widetilde{\sin\theta} \rangle$ is used to calculate the electromagnetic torque. The voltage output is given by the equation $e = \dot{\theta} M_F i_f \widetilde{\sin\theta}$ and the active and reactive power are defined from the equations $P = \dot{\theta} M_f i_f \langle i, \widetilde{\sin\theta} \rangle$ y $Q = -\dot{\theta} M_f i_f \langle i, \widetilde{\cos\theta} \rangle$, respectively. More details are available at [13].

The active power output is calculated and set from the frequency control loop within the synchroconverter control scheme [13]. This control is based on the difference between a virtual angular velocity ω and a reference velocity ω_r (interpreted as the nominal frequency of the network) [13], [2]. This difference is multiplied by a droop gain D_p, where the product represents the frequency droop mechanism to compensate for the difference between the mechanical torque T_m and the torque T_e, generated by the control equations [13], [2]. T_m is obtained from a reference active power P_r in the inverter and the angular velocity ω_r [13], [2]. In the control scheme J represents the virtual inertia of the synchronverter [13], [2]. Usually, the value of J is small so that the response of the control scheme is as fast as possible, since the time constant τ_f is inversely proportional to the inertia value, i.e. $\tau_f = J/D_p$. The frequency control loop is responsible for generating the phase angle (θ) of the the modulating signal for the PWM process [13], [2]. The dynamics of this control loop is based on the oscillation equation (Equation 5).

$$J\dot{\omega} = \frac{P_r}{\omega_r} - T_e - D_p(\omega - \omega_r) \tag{5}$$

Reactive power control is performed by voltage control loop, in this case by a virtual field excitation variable in the synchronverter [13], [2]. This control starts with the difference between a reference v_r (system base voltage) and a measured feedback voltage v_m at the filter capacitor terminals RLC. This difference is multiplied by the voltage drop coefficient D_q, similar to frequency control [13], [2]. The above product is added to the calculated reactive power error. The difference between the reference reactive power Q_r in synchronverter and the reactive power Q calculated by the control equations represents this error [13], [2]. Then the output of the described summation is added to the integrator with gain $1/K$ to modify $M_f i_f$, i.e., the virtual field current [13], [2]. Note that K (excitation gain) has an effect on the time constant τ_v as J in the frequency control loop. In the synchronverter, τ_v represents the time in which this inverter can supply reactive power to modify the voltage levels at its output [13], [2]. The dynamics of the voltage control loop are usually described using Equation 6.

$$M_f i_f = \frac{1}{K}[Q_r + D_q(v_r - v_m) - Q] \tag{6}$$

The single-line diagram of the synchroconverter used in this research is shown in the Fig. 4.

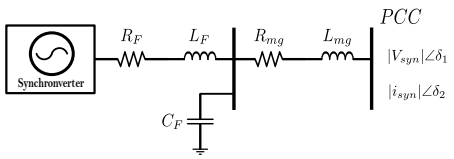

Fig. 4. Single-line diagram of the filter and line to the synchronverter output. [2].

Where $R_F = 0.042\Omega$, $L_F = 0.57 \times 10^{-3} H$ and $C_F = 1.56 \times 10^{-6} F$ represent the parameters of the filter RLC. R_{mg} y L_{mg} correspond to the data of the microgrid. $|V_{syn}|\angle\delta_1$ e $|i_{syn}|\angle\delta_2$ are the voltage and current measurements that are taken at the PCC that are required for the synchronverter.

The synchroconverter control parameters used in this research are shown in the Table II.

TABLE II
PROPOSED PARAMETERS OF THE SYNCHRONVERTER CONTROL STRUCTURE

Parameter	Symbol	Value
Coefficient of frequency control loop	D_p	14.7
Virtual inertia	J	0.2814
Coefficient of voltage control loop	D_q	5324.97
Excitation gain	K	40150.33

The objective of this research is to gradually replace each of the inverters in the microgrid (Fig. 1) with synchroconverters,

based on the topology of the microgrid, the inverter model and the proposed synchroconverter. The aim to analyze the dynamic behavior when synchronverter are added into the microgrid, studying the comparison between variables such as voltage, current, frequency, active power, and reactive power [14]. Since the synchronverter provides virtual inertia, it is expected that the dynamics of these variables will be more similar to those obtained when operating with synchronous generators. Therefore, it can be analyzed under what conditions and control laws in the converters improves or does not the performance in a microgrid. For this purpose, it is proposed to simulate three-phase and single-phase short-circuit events with different fault clearing times.

IV. Experiments

Based on the previous section, 4 case studies (A, B, C, and D) are presented. These scenarios consist in keeping the proposed microgrid topology and parameters, and only replacing the inverters with a conventional control law by synchronverters. Case studies are summarized in Table III. Case A corresponds exclusively to the system raised in Section II, where DG1, DG2 y DG3 are inverters with the control law described and shown in Fig. 2. In study case B, DG1 and DG3 are inverters and DG2 is the synchronverter described above and shown in Figs. 3 and 4. Case C, DG3 is an inverter and DG1 and DG2 are converters with the synchronverter function. In case D, all generating units in the microgrid are synchronverters.

TABLE III
Proposed Case Studies with Different Penetration of Inverters and Synchronverters

Generation unit	Case A	Case B	Case C	Case D
DG1	Inv	Inv	Syn	Syn
DG2	Inv	Syn	Syn	Syn
DG3	Inv	Inv	Inv	Syn

Inv: Conventional inverter
Syn:Synchronverter

The paper proposes 4 experiments consisting of the simulation of short-circuit events in the central bus of the microgrid, specifically where the loads $P = 0.05$ MW and $Q = 0.025$ MVAR are located, as shown in the Fig. 1. In these experiments, the fault is initiated at the second 1 and released; 1.66 ms, 9.66 ms and 16.66 ms later. The same event is reproduced for the 4 case estudies.

TABLE IV
Experiments for the 4 Case Studies under Different Fault Scenarios

Experiment	3F	1F	S/L	C/L
E1	✓		✓	
E2	✓			✓
E3		✓	✓	
E4		✓		✓

3F: three-phase short-circuit
1F: single-phase short-circuit
S/L: Without tripping of the faulted zone
C/L: With tripping of the faulted zone

Table IV summarizes the characteristics of the type of fault proposed in each of the experiments performed. Experiment E1 simulates a three-phase short-circuit without disconnection of the fault zone. E2 repeats the experiment carried out in E1, but with the disconnection of the zone in which the fault has occurred. This zone corresponds to the RL link that connects the buses where PCC1 and PCC3 are located. E3 corresponds to the simulation of a single-phase fault without disconnecting the faulted element. Finally, E4 simulates a single-phase short-circuit, but the faulted element is disconnected, i.e. the RL connection mentioned above is released.

V. Results

This section presents the results of the experiments performed. Voltage responses were measured on the common side of the AC bus, while currents were measured at the point of fault, with both variables expressed in RMS values. The operating frequency of the system is measured on the common bus. At the same time, the active and reactive power are measured at the output of the generating unit corresponding to PCC2. The case studies start from a steady-state obtained by simulating the system for 1 s. In addition, tables with simulation results for different fault release times are presented.

Fig. 5 shows the dynamic behavior of the electrical quantities as a result of Experiment E1, which consists of a three-phase short-circuit without tripping of the faulted zone. In 5a the voltage measured on the AC common bus is shown and it can be observed that the overshoot after the fault is higher in case A and B. When synchronverters are included in the microgrid (case C and D), the overshoot decreases. This behavior is attributed to the inertia introduced by the synchronverters. It is also observed that the response is slower, with a longer settling time, as would happen in a system dominated by synchronous machines. The steady-state error obtained from this simulation is shown in Table V. This error is given as a percentage and as a function of the RMS voltage, as expressed in Equation (7). It can be observed that as the number of synchronverters is increased, the steady state error is reduced.

$$e\% = \frac{v_i - v_f}{v_i} \times 100 \tag{7}$$

In Fig. 5b it is observed that the fault currents are similar in magnitude in all the cases considered. It can be observed that when there is a larger number of synchronverters, as in cases C and D, the maximum current values are reached in a shorter time. In these cases, it is also observed that there is a small contribution of short-circuit current after the fault has vanished. In 5c the frequency are shown and it is observed that the frequency deviations are higher when only inverters without inertia function are used (cases A and B). When synchronverters are introduced (cases C and D), these deviations decrease. Similarly, the frequency become slower as the number of synchronverters increases. Therefore, a lower ROCOF can be intuited when synchroconverters are introduced and a behavior more similar to a system dominated by synchronous generators. The maximum and minimum values reached by the operating frequency during the simulated

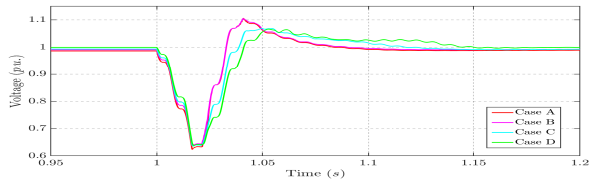

(a) Dynamic response of RMS voltage on the common bus: case A (—), case B (—), case C (—), case D (—).

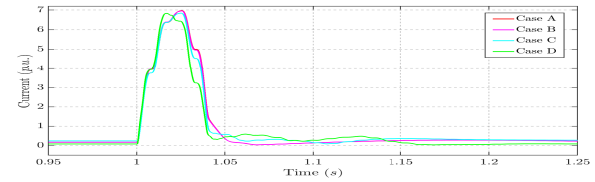

(b) Dynamic response of short-circuit RMS current: case A (—), case B (—), case C (—), case D (—).

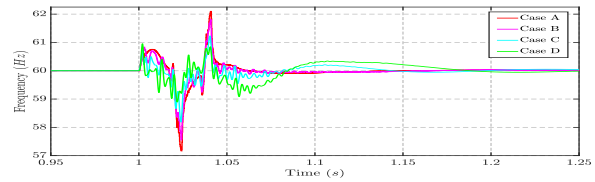

(c) Dynamic frequency response on the common bus: case A (—), case B (—), case C (—), case D (—).

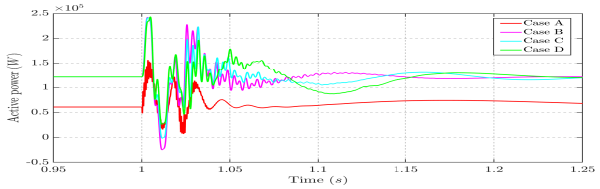

(d) Dynamic response of the active power at the output of DG2: case A (—), case B (—), case C (—), case D (—).

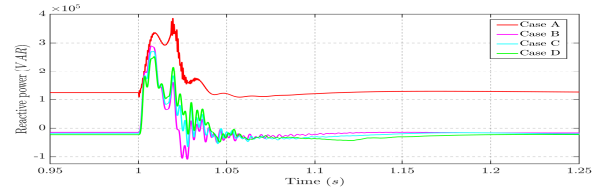

(e) Dynamic response of the reactive power at the output of DG2: case A (—), case B (—), case C (—), case D (—).

Fig. 5. Experiment E1 (three-phase temporary fault) with failure clearing time of 16.66 ms.

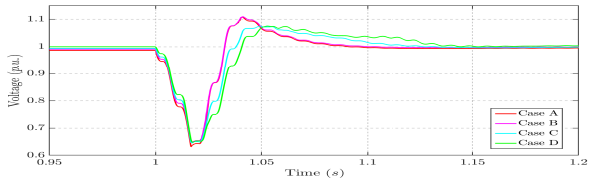

(a) Dynamic response of RMS voltage on the common bus: case A (—), case B (—), case C (—), case D (—).

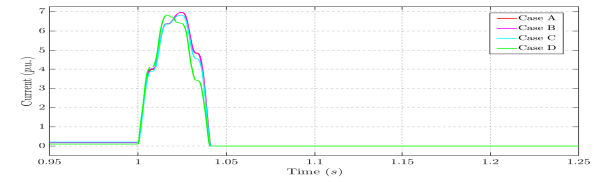

(b) Dynamic response of short-circuit RMS current: case A (—), case B (—), case C (—), case D (—).

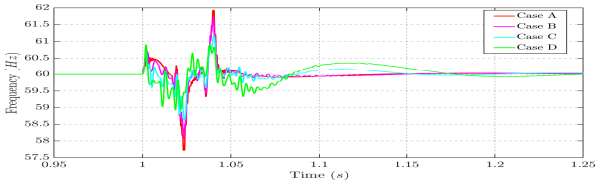

(c) Dynamic frequency response on the common bus: case A (—), case B (—), case C (—), case D (—).

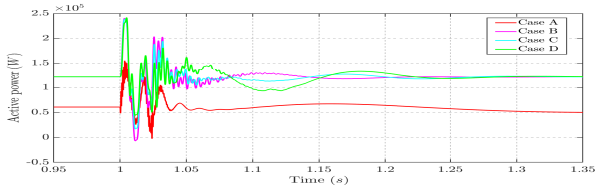

(d) Dynamic response of the active power at the output of DG2: case A (—), case B (—), case C (—), case D (—).

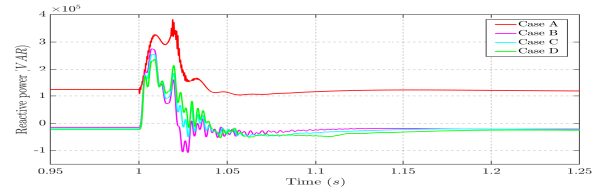

(e) Dynamic response of the reactive power at the output of DG2: case A (—), case B (—), case C (—), case D (—).

Fig. 6. Experiment E2 (three-phase fault with PCC1 to PCC3 disconnected) with failure clearing time of 16.66 ms.

short-circuit are shown in Table VI. This is shown for different fault clearing times. It is observed that as the number of synchronverters in the microgrid increases, the peak frequency values deviate less from the nominal frequency of the system, in this case 60 Hz.

Figs. 5d and 5e show the dynamic responses of the active and reactive power supplied by DG2. In both figures, as in the case of currents, voltages and frequencies, the dominant dynamics of the responses are of lower frequency as the number of synchronverters in the system increases.

Fig. 6 shows the system dynamics resulting from E2. In 6a the RMS voltage, also measured on the AC common bus, is plotted. It is observed that with the inclusion of synchronverters, both the overshoot and the voltage drop decrease, which is associated with a greater change in the reactive power injected by the synchronverters under the short-circuit condition. Fig. 6b shows the short-circuit current and it can be observed that the dynamics presented is similar to the behavior described in the E1. In this case, it can be seen that there is not current contribution after the fault is cleared, since the zone where the fault occurs is disconnected. The frequency oscillations of Experiment 2 are shown in 6c, it can be seen that the deviations are smaller compared to the first experiment. In numerical terms, this can also be seen in the simulation results shown

in the Table VII. Note that both the maximum and minimum values deviate less from the operating frequency of 60 Hz.

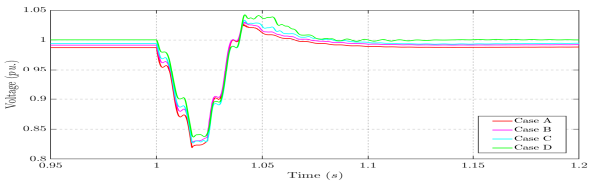

(a) Dynamic response of RMS voltage on the common bus: case A (—), case B (—), case C (—), case D (—).

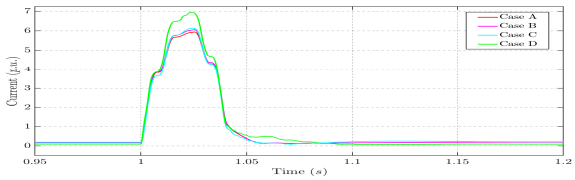

(b) Dynamic response of short-circuit RMS current: case A (—), case B (—), case C (—), case D (—).

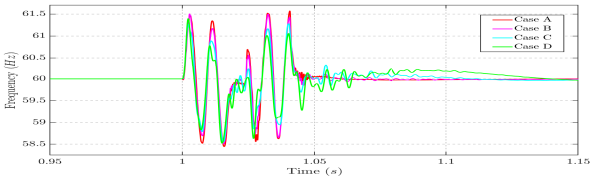

(c) Dynamic frequency response on the common bus: case A (—), case B (—), case C (—), case D (—).

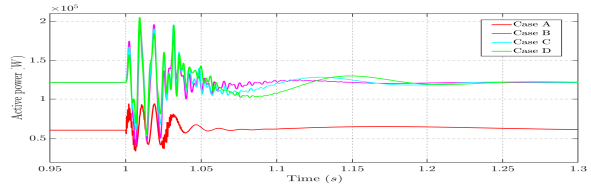

(d) Dynamic response of the active power at the output of DG2: case A (—), case B (—), case C (—), case D (—).

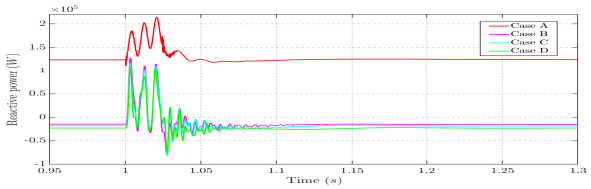

(e) Dynamic response of the reactive power at the output of DG2: case A (—), case B (—), case C (—), case D (—).

Fig. 7. Experiment E3 (single-phase temporary fault) with failure clearing time of 16.66 ms.

Figs. 7 and 8 show the results for the same variables as those presented for the three-phase fault case (Figs. 5 and 6), but now for a single-phase fault on the same bus. Fig. 7 refers to the responses to the temporary single-phase fault. Fig. 8 refers to the responses to a single-phase fault where the lines from PCC1 to PCC3 are disconnected to clear the fault. In both experiments, the fault clearing time of one network cycle is considered.

Compared to the transient three-phase fault (E1, Fig. 5a), the voltage drop and settling times are lower for the transient

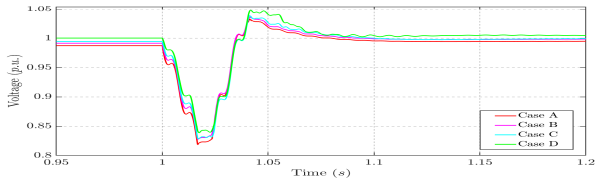

(a) Dynamic response of RMS voltage on the common bus: case A (—), case B (—), case C (—), case D (—).

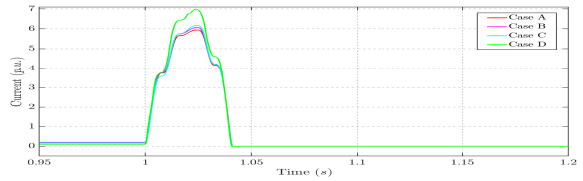

(b) Dynamic response of short-circuit RMS current: case A (—), case B (—), case C (—), case D (—).

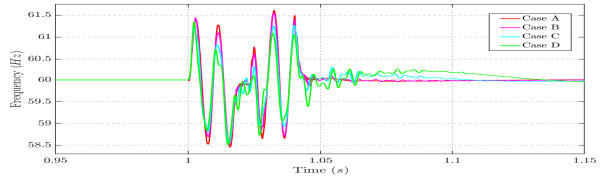

(c) Dynamic frequency response on the common bus: case A (—), case B (—), case C (—), case D (—).

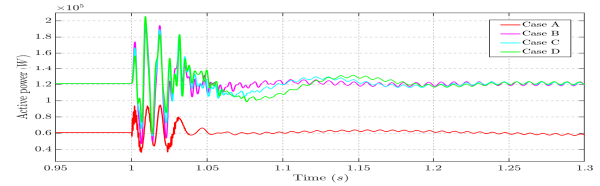

(d) Dynamic response of the active power at the output of DG2: case A (—), case B (—), case C (—), case D (—).

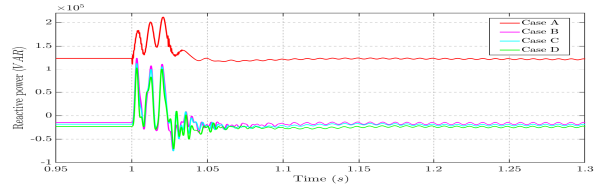

(e) Dynamic response of the reactive power at the output of DG2: case A (—), case B (—), case C (—), case D (—).

Fig. 8. Experiment E4 (single-phase fault with PCC1 to PCC3 disconnected) with failure clearing time of 16.66 ms.

single-phase fault (E3, Fig. 7a); both results are expected because the single-phase fault is less severe than the three-phase fault. The short-circuit current of the single-phase fault is lower than that of the three-phase fault, except in case D, where all the converters have the synchronverter function. This behavior is the same for both temporary and permanent single-phase faults, E3 and E4, respectively (Figs. 7b y 8b).

The frequency deviations for the single-phase fault are smaller than those for the three-phase fault. This result is also expected because the single-phase fault is less severe than the three-phase fault. It is observed that the frequency deviations are smaller as the number of inverters with the

synchronverter function increases. Similarly, the effect of the increase in total inertia of these inverters is reflected in the appearance of lower frequency oscillations, as in the case of synchronous generators. This behavior can also be observed in the active and reactive powers supplied by the inverters with synchronous converter function, in particular Figs. 7d, 8d and 7e, 8e, respectively, and supplied by DG2. Note that as expected, less active and reactive power is delivered for the single-phase fault than for the three-phase fault.

TABLE V
E1 VOLTAGE STEADY-STATE ERROR WITH A TEMPORALLY THREE-PHASE SHORT-CIRCUIT EVENT DURING 1.66MS, 9.16 MS AND 16.66 MS, RESPECTIVELY, (%)

Case	1.66 ms	9.16 ms	16.66 ms
Case study A	-8.16×10^{-2}	-1.68×10^{-1}	-2.84×10^{-1}
Case study B	-9.90×10^{-2}	-1.90×10^{-1}	-3.08×10^{-1}
Case study C	-3.98×10^{-2}	-6.99×10^{-2}	-9.97×10^{-2}
Case study D	-5.32×10^{-8}	-3.01×10^{-8}	2.55×10^{-8}

TABLE VI
E1 FREQUENCY DEVIATIONS WITH A TEMPORARY THREE-PHASE SHORT-CIRCUIT EVENT, (HZ)

FCT	1.66 ms		9.16 ms		16.66 ms	
Model/Freq	Max	Min	Max	Min	Max	Min
Case A	61.88	58.02	61.97	58.05	62.05	57.19
Case B	61.64	58.17	61.65	58.37	61.75	57.64
Case C	61.61	57.88	61.41	58.41	61.22	58.18
Case D	61.80	58.05	61.39	58.22	60.95	58.89

TABLE VII
E2 FREQUENCY DEVIATIONS WITH THE DISCONNECTION FROM PCC1 TO PCC3 DUE TO A THREE-PHASE SHORT-CIRCUIT EVENT, (HZ)

FCT	1.66 ms		9.16 ms		16.66 ms	
Model/Freq	Max	Min	Max	Min	Max	Min
Case A	61.73	58.23	61.75	58.34	61.93	57.70
Case B	61.57	58.43	61.69	58.38	61.72	58.06
Case C	61.63	58.33	61.46	58.54	61.19	58.61
Case D	61.67	58.29	61.25	58.57	60.90	58.92

TABLE VIII
E3 VOLTAGE STEADY-STATE ERROR WITH A TEMPORALLY SINGLE-PHASE SHORT-CIRCUIT EVENT, (%).

Case	1.66 ms	9.16 ms	16.66 ms
Case study A	-3.17×10^{-2}	-6.33×10^{-2}	-9.56×10^{-2}
Case study B	-4.68×10^{-2}	-8.03×10^{-2}	-1.14×10^{-1}
Case study C	-2.43×10^{-2}	-3.47×10^{-2}	-4.53×10^{-2}
Case study D	-5.72×10^{-8}	8.66×10^{-8}	-2.62×10^{-8}

To evaluate the effect of fault clearance time, Tables V, VI, VII, VIII, IX y X are presented. The steady-state error of Experiments 1 and 3, respectively, are shown in Tables V and VIII. Both experiments consist of the temporally cleared fault. It is observed that as the number of synchronverters increases (case D), this error decreases significantly compared to cases (A, B and C). This could be attributed to the increased inertia provided by the synchronverters. The maximum and minimum frequencies reached at the different fault clearing times evaluated are shown in Tables VI and VII. This is for the temporary three-phase short-circuit event and with fault clearing, respectively. It is observed that as synchroconverters are introduced, the frequency deviations are smaller. It is also observed that these deviations are smaller when the fault zone is released, as shown in Table VII of Experiment E2, compared to that of Experiment E1 (Table VI). The maximum and minimum frequency values reached when simulating a single-phase fault are shown in Tables IX and X. A behavior similar to that described for the three-phase fault is observed, since the frequency deviations are smaller as the number of synchronizers increases and the fault zone is cleared. It is also observed that the maximum and minimum frequency values reached during the single-phase short-circuit deviate less from the nominal frequency of 60 Hz compared to the three-phase fault.

TABLE IX
E3 FREQUENCY DEVIATIONS WITH A TEMPORARY SINGLE-PHASE SHORT-CIRCUIT EVENT, (HZ)

FCT	1.66 ms		9.16 ms		16.66 ms	
Model/Freq	Max	Min	Max	Min	Max	Min
Case A	61.48	58.46	61.53	58.38	61.57	58.44
Case B	61.50	58.50	61.50	58.49	61.50	58.50
Case C	61.27	58.82	61.40	58.55	61.28	58.55
Case D	61.39	58.74	61.40	58.28	61.40	58.51

TABLE X
E4 FREQUENCY DEVIATIONS WITH THE DISCONNECTION FROM PCC1 TO PCC3 DUE TO A SINGLE-PHASE SHORT-CIRCUIT EVENT, (HZ)

FCT	1.66 ms		9.16 ms		16.66 ms	
Model/Freq	Max	Min	Max	Min	Max	Min
Case A	61.42	58.59	61.53	58.52	61.61	58.45
Case B	61.44	58.63	61.44	58.60	61.56	58.50
Case C	61.63	58.33	61.46	58.54	61.19	58.61
Case D	61.67	58.29	61.25	58.57	60.90	58.92

VI. CONCLUSION

This paper presents experiments on a microgrid with traditional inverter control and synchronverters. It simulates three-phase and single-phase short circuits with fault zone tripping and non-tripping on a microgrid bus. The simulations, conducted in MATLAB/Simulink, maintain the microgrid's characteristics, topology, and fault clearing time, revealing the following outcomes:

- In the transient process during the fault event simulation, it is observed that the frequency oscillations are slower when inverters with the synchroconverter function are introduced. The frequency deviations are also smaller.
- When synchronverters are introduced into the microgrid, power oscillations also decrease.
- When synchronverters are added to the microgrid, after the fault occurs and is cleared, the voltage response to return to steady-state is slower and the steady-state error is lower.

- During the fault event simulation, voltage sags and overshoots at the fault point decrease as synchronverters are introduced.

Through the analysis of the cases and experiments presented, it has been shown that the dynamic behavior between symmetrical and asymmetrical short-circuit events in a microgrid can be different when synchronverters and/or inverters are used. However, it has been shown that the gradual increase in the number of units with the synchroconverter function has a positive effect on the operating frequency of a microgrid.

Future work involves simulating load changes, measuring ROCOF, analyzing dynamic behavior in larger microgrids, and real-time experimental implementation.

REFERENCES

[1] L. Mehigan, D. Al Kez, S. Collins, A. Foley, B. Ó'Gallachóir, and P. Deane, "Renewables in the european power system and the impact on system rotational inertia," *Energy*, vol. 203, p. 117776, 2020. https://doi.org/10.1016/j.energy.2020.117776.

[2] J. Segundo Ramírez, J. Hernández Ramírez, N. Visairo Cruz, and R. Peña Gallardo, "Bifurcation stability analysis of the synchronverter in a microgrid," *Energies*, vol. 15, no. 21, 2022. https://doi.org/10.3390/en15217992.

[3] P. Piya and M. Karimi-Ghartemani, "A stability analysis and efficiency improvement of synchronverter," in *2016 IEEE Applied Power Electronics Conference and Exposition (APEC)*, pp. 3165–3171, IEEE, 2016. https://doi.org/10.1109/apec.2016.7468317.

[4] N. Hatziargyriou, J. Milanovic, C. Rahmann, V. Ajjarapu, C. Canizares, I. Erlich, D. Hill, I. Hiskens, I. Kamwa, B. Pal, *et al.*, "Definition and classification of power system stability–revisited & extended," *IEEE Transactions on Power Systems*, vol. 36, no. 4, pp. 3271–3281, 2020. https://doi.org/10.1109/tpwrs.2020.3041774.

[5] G. Barzilai, L. Marcus, and G. Weiss, "Energy storage systems—grid connection using synchronverters," in *2016 IEEE International Conference on the Science of Electrical Engineering (ICSEE)*, pp. 1–5, IEEE, 2016. https://doi.org/10.1109/icsee.2016.7806095.

[6] G. Lalor, J. Ritchie, S. Rourke, D. Flynn, and M. J. O'Malley, "Dynamic frequency control with increasing wind generation," in *IEEE Power Engineering Society General Meeting, 2004.*, pp. 1715–1720, IEEE, 2004. https://doi.org/10.1109/pes.2004.1373170.

[7] P. Tielens, S. De Rijcke, K. Srivastava, M. Reza, A. Marinopoulos, and J. Driesen, "Frequency support by wind power plants in isolated grids with varying generation mix," in *2012 IEEE Power and Energy Society General Meeting*, pp. 1–8, IEEE, 2012. https://doi.org/10.1109/pesgm.2012.6344690.

[8] M. Rezkalla, M. Pertl, and M. Marinelli, "Electric power system inertia: Requirements, challenges and solutions," *Electrical Engineering*, vol. 100, pp. 2677–2693, 2018. https://doi.org/10.1007/s00202-018-0739-z.

[9] H.-P. Beck and R. Hesse, "Virtual synchronous machine," in *2007 9th international conference on electrical power quality and utilisation*, pp. 1–6, IEEE, 2007. https://doi.org/10.1109/epqu.2007.4424220.

[10] M. Van Wesenbeeck, S. De Haan, P. Varela, and K. Visscher, "Grid tied converter with virtual kinetic storage," in *2009 IEEE Bucharest PowerTech*, pp. 1–7, IEEE, 2009. https://doi.org/10.1109/ptc.2009.5282048.

[11] J. M. Guerrero, L. G. De Vicuna, J. Matas, M. Castilla, and J. Miret, "A wireless controller to enhance dynamic performance of parallel inverters in distributed generation systems," *IEEE Transactions on power electronics*, vol. 19, no. 5, pp. 1205–1213, 2004. https://doi.org/10.1109/tpel.2004.833451.

[12] U. Tamrakar, D. Shrestha, M. Maharjan, B. P. Bhattarai, T. M. Hansen, and R. Tonkoski, "Virtual inertia: Current trends and future directions," *Applied sciences*, vol. 7, no. 7, p. 654, 2017. https://doi.org/10.3390/app7070654.

[13] Q.-C. Zhong and G. Weiss, "Synchronverters: Inverters that mimic synchronous generators," *IEEE transactions on industrial electronics*, vol. 58, no. 4, pp. 1259–1267, 2010. https://doi.org/10.1002/9781118481806.ch18.

[14] F. Katiraei, M. R. Iravani, and P. W. Lehn, "Micro-grid autonomous operation during and subsequent to islanding process," *IEEE Transactions on power delivery*, vol. 20, no. 1, pp. 248–257, 2005. https://doi.org/10.1109/pes.2004.1373266.

[15] G. Agundis-Tinajero, J. Segundo-Ramírez, N. Visairo-Cruz, M. Savaghebi, J. M. Guerrero, and E. Barocio, "Power flow modeling of islanded ac microgrids with hierarchical control," *International Journal of Electrical Power & Energy Systems*, vol. 105, pp. 28–36, 2019. https://doi.org/10.1016/j.ijepes.2018.08.002.

[16] J. Rocabert, A. Luna, F. Blaabjerg, and P. Rodriguez, "Control of power converters in ac microgrids," *IEEE transactions on power electronics*, vol. 27, no. 11, pp. 4734–4749, 2012. https://doi.org/10.1109/tpel.2012.2199334.

[17] Q. Shafiee, J. M. Guerrero, and J. C. Vasquez, "Distributed secondary control for islanded microgrids—a novel approach," *IEEE Transactions on power electronics*, vol. 29, no. 2, pp. 1018–1031, 2013. https://doi.org/10.1109/tpel.2013.2259506.

[18] Y. Zhang, S. Wu, P. Yang, S. Xiang, S. Li, and S. He, "Research on parallel operation of virtual synchronous generators in microgrid," in *2019 14th IEEE Conference on Industrial Electronics and Applications (ICIEA)*, pp. 1659–1664, IEEE, 2019. https://doi.org/10.1109/iciea.2019.8833673.

[19] S. Wang, R. Qi, and Y. Li, "Fuzzy control scheme of virtual inertia for synchronverter in micro-grid," in *2018 21st International Conference on Electrical Machines and Systems (ICEMS)*, pp. 2028–2032, IEEE, 2018. https://doi.org/10.23919/icems.2018.8549309.

[20] P. Piya and M. Karimi-Ghartemani, "A stability analysis and efficiency improvement of synchronverter," in *2016 IEEE Applied Power Electronics Conference and Exposition (APEC)*, pp. 3165–3171, IEEE, 2016. https://doi.org/10.1109/apec.2016.7468317.

Cristian Hernández-García received a graduate in electrical engineering from Universidad Veracruzana and obtained the M.Sc in Electrical Power Systems from the Universidad Autónoma de San Luis Potosí. Since 2019, he has currently works as a part-time professor at Universidad Veracruzana. His research interests are inertia in electrical power systems, virtual inertia and simulation.

Juan Segundo-Ramírez (M'10) received the M.Sc. degree from the CINVESTAV Guadalajara, Zapopan, Mexico, in 2004, and the Ph.D. degree from the Universidad Michoacana de San Nicolas de Hidalgo, Michoacán, México, in 2010, both in electrical power systems. Since 2010, he has been with the Universidad Autónoma de San Luis Potosí, San Luis Potosí, México. His research interests include power system harmonic analysis, modeling, design, and simulation.

Nancy Visairo-Cruz received a graduate degree in Electronic Engineering from the Technologic Institute of Oaxaca, México in 1997. She received the M. S. and Ph. D degrees specializing in Automatic Control from the National Center of Research and Technological Development, Cuernavaca, Mexico in 1999 and 2004, respectively. Since 2005 she has been working as a professor-researcher at the Center for Research and Graduate Studies of the Faculty of Engineering of the Autonomous University of San Luis Potosi. She is a member of the National Research System at Level 1. Among her topics of interest are automatic control schemes for power electronics systems applied to power quality, electric vehicles, renewable energy, and storage systems. She is also interested in fault diagnosis topics in energy storage systems.

Jesús Camarillo-Montero received the M.Sc degree in energy engineering from the Universidad Veracruzana and PhD in engineering from Universidad Martí. Since 2012, he currently works as a full-time lecturer at the Universidad Veracruzana. Also, he is the Secretary of the Power and Energy Society Chapter (PES) of the IEEE Veracruz Section. His research interests are energy savings, electric load models and voltage optimization.